Demulsification of crude oil emulsions tracked by pulsed field gradient NMR. Part II: Influence of chemical demulsifiers in external AC electric field

Tomas Nordeide Hjartnes*[1], Sameer Mhatre[1], Bicheng Gao[1], Geir Humborstad Sørland[2], Sébastien Simon*[1], Johan Sjöblom[1]

[1] Ugelstad Laboratory, Department of Chemical Engineering, Norwegian University of Science and Technology (NTNU), N-7491 Trondheim, Norway
[2] Anvendt Teknologi AS, Munkvollveien 56, 7022 Trondheim, Norway

*Corresponding authors at: Department of Chemical Engineering, Ugelstad Laboratory, NTNU, N-7491 Trondheim, Norway
E-mail adresses: tomas.hjartnes@ntnu.no (T. Hjartnes), sebastien.c.simon@ntnu.no (S. Simon)

Abstract

Crude oil emulsions can reach stability levels that pose severe challenges for the processing industry. Certain conventional methods are used to deal with these challenges, such as chemical demulsification. In this article, two chemicals were mixed with crude oil emulsions to study their separation capabilities in the presence and absence of external AC fields. Experiments were conducted at 65 ^{o}C to lower crude oil viscosity, which in turn affects separation efficiency. Effects from the chemical and electrical constituents on the crude oil emulsion was tracked by a pulsed field gradient NMR method, developed in a previous study. The NMR measured emulsified water content for 2 hours, continuously, as a function of sample height. Given the water content, droplet sedimentation and free water layer kinetics could be quantified. Droplet size distributions from the top half oil phase were obtained at the beginning and end of each experiment, with the intent of mapping coalescence and sedimentation development of droplets. However, tracking droplet size evolution proved challenging due to rapid changes within the emulsion. The main focus with the NMR technique was therefore on sedimentation and free water layer kinetics. A synergy was observed between the two chemicals and low AC fields. The two chemicals showed varied degrees of separation efficiency, where limited amounts of water was resolved by chemical 1 without electric field, though it improved separation past the limit of electrical treatment when used in combination with AC field. Above a given electric field, sedimentation by electrocoalscence dominates, and the effect of chemical demulsifier is marginal. Chemical 2 achieved promising results as a lone separation method, while further enhancing separation in collaboration with AC fields. Chemical 1 was inefficient in the absence of field, but worked well to remove small droplets in combination with AC field.

1. INTRODUCTION

One of the most fundamental problems faced within the oil industry, when processing crude oil, is the removal of production and formation water dispersed within the oil. These mixtures are referred to as emulsions, which are thermodynamically unstable [1]. Water separation from such emulsions is a necessity, both from a practical and economic standpoint, as it promotes higher oil quality, prevents corrosion of equipment and reduces energy requirements during transport. The water contents in export oil should not exceed 0.5% by weight. In other cases there will be economic consequences [2]. Water-in-crude oil emulsions are commonly dealt with during production, while crude oil-in-water emulsions most often occur in the form of production water [3]. The main challenges with water-in-crude oil emulsions are the many components within the crude oil, which serve as stabilizing agents for the dispersed water droplets, particularly the asphaltene aggregates solvated by resins [4]. Therefore, a more potent driving force is usually needed besides gravity to make droplets coalesce.

A variety of techniques are available for water separation, but only a few are selected for practical implementation based on efficiency and cost. Extensive reviews [5-8] have been written to cover different advantages and drawbacks of the many existing methods. Besides gravity separation [9], these processes include addition of chemical demulsifiers [10], heating of crude oil [3], electrocoalescence [11], liquid membrane separation [12], biological demulsifiers (bacterial growth) [13] and microwave irradiation [14]. Amongst these, electrocoalescence has been an actively studied subject parallel to its application development [15-18] since the origin of the electrostatic precipitator under Cottrell and Speed [19]. Electrocoalescence aims to coalesce water droplets in an emulsion by polarizing them, resulting in attraction and merging of droplets that subsequently sediment out by gravity. The advantage of using this method over others, such as heating or centrifugation, is its reduced energy consumption. However, a possible disadvantage of this method is the formation of fine droplets that snap off of larger droplets after these coalesce during field application on a water-in-oil emulsion. This appearance of secondary droplets was illustrated for a DC field, resulting from a typical Taylor cone [7]. These Taylor cone formations occur on droplets in the form of conical protrusions when field strengths become too high. As the cone snaps, it leaves several smaller dispersed droplets behind.

Another well established method is the use of chemical demulsifiers to modify the properties of complex crude oil systems [1, 10, 20-23], and more easily achieve drop-drop coalescence when droplets collide through Brownian motion, turbulence or sedimentation. Both aforementioned techniques are often used in the presence of elevated temperatures to reduce the viscosity of the oil and increase droplet velocity, thus promoting coalescence.

Earlier research in the field of electrocoalescence focused on understanding basic mechanisms at play between closely spaced droplets in uniform DC fields. Pearce [24] observed that the electrical treatment of emulsions occur in two steps in concentric electric fields. Firstly, that droplets align into chains, and secondly that adjacent droplets coalesce to a point when they can sediment. He also suggested that droplet diameters smaller than a certain size puts a constraint on their ability to coalesce into larger droplets during electric field. A study by Berg [25] concluded that delay of coalescence of liquid drops in contact is dependent on applied voltage strength across the droplets. Indicated from his experiments, coalescence rates, v_1 and v_2, are proportional to μV at low voltages and to V^2 at high voltages, respectively:

$$v_1 = k_1 \mu V \quad (1)$$

$$v_2 = k_2 \varepsilon V^2, \quad (2)$$

where k_1 and k_2 are experimentally determined constants with capacitance C. μ is the dipole moment of the intermolecular bonds, ε is the dielectric constant and V is the voltage. Similar observations were made by Sartor [26], in which coalescence of droplets falling through mineral oil directly correlates to strength of applied electrical field.

Electrocoalescence and chemical additives have been widely investigated individually, but limited focus on combining them [27-29]. Treating emulsions with chemicals before subjecting them to electric field was first proposed in a patent by Eddy [16]. His findings suggested that the chemical altered the physical properties of the emulsion, allowing for application of electric field at lower temperatures than in the absence of such chemicals. Less [27] reported significant improvements and faster separation during combined AC electric field and chemicals to treat water-in-oil emulsions compared to using chemicals only. The use of DC electric field has been studied in combination with several different demulsifiers by Mhatre [28] to characterize critical electric fields of crude oil emulsions. The critical electric field describes the electric potential at which point the water-oil interface becomes unstable, inducing drop-drop contact by deformation or bridging of droplets [28]. The results of Mhatre pointed towards an existing threshold for maximum demulsifier concentration, at which no further separation increase was achieved with the combined use of field and chemical. It was also found by Mhatre that the addition of demulsifier before emulsification generated better results compared to adding demulsifier after emulsification. A similar set-up for DC electric field was investigated by Yang [29], where the critical field strength was shown to reduce with addition of a chemical. This indicated that partial droplet coalescence was promoted by the resulting decrease of interfacial tension.

Previous studies on demulsification of emulsions have used various visualization tools to quantify droplet coalescence and sedimentation mechanisms. Bottle testing [10] is an extensively used method solely based on visual inspection of a graded cylinder to obtain data on water resolution. Multiple dynamic light scattering [30] is a method for studying demulsifier behavior and mechanisms during emulsion destabilization. Microfluidics has widespread applications, amongst these to study fusion of emulsified droplets inside micro channels by AC electric fields [32], as well as mechanisms of drop coalescence by chemical demulsifiers [31]. Sample opaqueness, such as in the case for crude oil, has put constraints on many of the aforementioned characterization techniques. This issue is circumvented by use of Pulsed Field Gradient (PFG) Nuclear Magnetic Resonance (NMR). The PFG NMR can trace the hydrogens in the water phase inside the dark crude oil, and thereby the water content, rapidly and without invasiveness [32].

This article is a follow-up on a series aiming to improve oil-water separation in production separators. In part I [33], an NMR method was developed and applied to study the mechanisms of chemical demulsifiers in absence of electric field. In part II, the same NMR method (as part I) will be implemented to study the synergy between chemical demulsification and electrocoalescence. In particular, it will be investigated if limitations of separation efficiency, encountered by the use of each method separately, may be overcome by combining them. For this purpose, two previously studied chemical demulsifiers from part I will be considered.

2. THEORY

The 3 stages of electrocoalescence

Electrocoalescence has been applied successfully for separation of water-in-crude oil emulsions since its invention. There have been several proposed mechanisms as the main driving forces behind droplet coalescence by use of electric field. Such driving forces lead to coalescence between two droplets occurring in three stages [5]. The first step is where the external field induces a positive and negative charge on opposite ends of a droplet in alignment with the field. Droplet-ends of opposite polarity will

then attract to each other through electrostatic forces. In the second step, as droplets come closer, the continuous thin oil film is squeezed out from in-between the droplets (film drainage). Rate of film thinning is dependent on the capillary pressure across the water and oil phases and the disjoining pressure. If a surfactant is present at the interface the Marangoni effect, referring to the presence of an interfacial tension gradient, also dampen the rate of film thinning [6]. At the third step, the thin film reaches a critical point of rupturing in which the droplets come in direct contact, becoming an area of high localized field strength [34], followed by coalescence.

Forces and mechanisms

There are numerous forces involved in causing the movement and retardation of emulsified droplets during electric field application. The main forces exerted on emulsified droplets by electric field are [11]: *(a) Dipole-dipole forces*. These result from an electric field, causing droplets to attract each other by polarizing the liquid of neutral charge so that the droplet receives opposite charges of equal magnitude at each end, aligned with the field direction. Droplet size and spacing dictates the force of attraction between droplets. Dipole-dipole forces are the predominant reason for droplet coalescence during electrostatic emulsion treatment, as this force directly causes droplet attraction. (b) *Electrophoretic forces*. The droplets receive a net electric charge that causes them to move in or opposite the direction of the field. This force does not promote droplet attraction, but merely relies on random collision for coalescence. It occurs during DC field application, but does not play a role in AC fields. (c) *Dielectrophoretic forces*. In a non-uniform external electric field, these forces act on droplets of neutral charge. A field gradient results from the non-uniform field which polarizes the droplets unevenly so that they are driven in a certain direction, depending on electric conductivities and permittivities of the liquid phases [35]. No attraction is induced between droplets themselves.

As the electrostatic and gravity forces set the droplets in motion, they experience *drag forces* that result from the viscosity of the continuous medium, retarding the movement of droplets, which can be described by Stokes' drag law [11]:

$$f_d = 6\pi\mu r u, \tag{3}$$

where μ is the viscosity of the oil, r is the droplet radius and u is the droplet velocity through the oil.

Once two droplets have moved close enough, and the thin film reduces to a certain distance, van der Waals forces will start taking effect in the attraction at an intermolecular level. At the same time, the electrical double layer has a repulsion effect between the same molecules that oppose the droplet attraction. Below a critical thickness, the thin film ruptures and the droplets coalesce. Pearce [24] suggested that droplet coalescence is driven by a force arising from induced charges on the droplets or electrical breakdown of the thin film layer between droplets once the field strength reaches a certain value. Thresholds for electric field strengths have also been shown to exist in which droplet break up reduces coalescence efficiency [6]. Rate of coalescence was proposed by Berg [25] to depend on the making and breaking, as well as reorientation, of bonds across the interfaces of contacting droplets. The thin films have been found to exhibit two types of behavior [34], referred to as type I and type II. When the thin film is incompressible it is of type I, as is the case when droplets are covered in by asphaltene aggregates in the form of a visco-elastic layer, as discussed by Kilpatrick et al [4]. This leads to an increase of emulsion conductivity as drop-drop coalescence is inhibited, promoting chain formation of droplets instead. Type II is the contrary, when the thin film is compressible, such as in the presence of surfactants at the droplet interface. The emulsion conductivity is limited for this case.

Effect of electric field forms

Various forms of electric field have been investigated for oil-water separation by electrical treatment, the most common being direct current (DC) [36], alternating current (AC) [2], pulsed DC [37, 38] or the aforementioned wave forms combined [39]. Because of the droplet alignment, and subsequent short-circuit often experienced by DC field; pulsed DC and AC have often been used to treat emulsions with high water content [6]. Long droplet chain formation has been observed at low frequencies in pulsed wave forms, while short chains were observed at high frequencies up to 1 kHz [40]. A sudden electrostatic discharge, caused by droplet chains, can be circumvented by electrode insulation (in case of DC) or increase of frequency (in case of AC). At higher frequency, droplets are given less time to respond, reducing chances of short-circuiting between uncoated electrodes. However, the potential difference across the electrodes becomes significantly reduced by introducing a dielectric material. This loss of potential across insulation is far less when using a time-varied electric field than for a DC field. In addition, the ions within the dispersed water droplets have less time to move towards the electrodes, thereby reducing corrosion, when using AC or pulsed DC as opposed to DC [35]. Because of the potential loss across electrode insulation, differences in the behaviors between various pulsed wave forms (square, half-wave, triangular, etc.) become reduced to the effects similar to a regular sinusoidal wave.

The use of pulsed DC was first investigated by Bailes and Larkai [41]. Mechanisms in pulsed DC, leading to drop-drop coalescence, were suggested to be very different from constant DC. Droplets in pulsed DC are propelled towards one another in random collisions, induced by repeated formation and breakdown of chains. They found an existing optimum frequency depending on the electrode coating thickness and given emulsion system. Pulsed DC has since been the focus of a wide range of research [38, 42-44]. Lesaint [45] has shown the importance of choosing the appropriate waveform. By comparing different AC signals, the square waveform was found to be most efficient, followed by sinusoidal and then triangular. Applying an alternating current (AC) field to a water-in-oil emulsion involves two particular phenomena [34]: (1) Droplet deformation and (2) drop-drop attraction. Both cases result from induced droplet charges by field polarization. Once a droplet is subjected to an external electric field in the first case, its shape will deform and become elongated in the shape of a prolate spheroid as a result of the electric stresses exerted on it.

Frequency in sinusoidal fields has shown variability in separation efficiency, suggesting a strong relation between experimental set-ups used for investigation and optimal frequency [2]. Research has shown that in order to find an optimum frequency, when dealing with coated electrodes, the duration of one half period of applied voltage must be short compared to the oil time constant, τ, expressed as [46]:

$$\tau = \frac{\varepsilon}{\gamma} \tag{4}$$

where ε is the permittivity and γ is the conductivity of the oil phase surrounding the droplets.

Using a high voltage in combination with a high frequency has displayed high coalescence frequency of droplets [47]. However, it has also lead to charge exchange between droplets that then repel each other. Reducing the voltage while keeping a high frequency resolved this issue.

3. METHODS

3.1. Fluids and chemicals

Crude oil emulsions consist of a North Sea heavy crude oil and 3.5% synthethic brine, mixed to give 50% oil volume. The North Sea heavy crude oil was provided by Equinor, which was used during all experiments reported in this article. All of its characteristics are listed in Table 1. Chemical demulsifiers used were provided by Nouryon (previously AkzoNobel) and NalcoChampion, with their characteristics in Table 2. The same demulsifiers were subject of another study [33], and concentrations used in this experimental work are therefore chosen based on their previously observed performance.

Table 1: Characteristics of the North Sea heavy crude oil used for emulsion generation in all experiments.

						SARA analysis [48]			
Density at 15 °C (g/cm3)	**Density at 65 °C (g/cm3)**	**Viscosity at 65 °C (mPa·s)**	**TAN (mg·g-1)**	**TBN (mgKOH· g-1)**	**Wat. cont.[a] (%)**	**Saturates (wt %)**	**Aromatics (wt %)**	**Resins (wt %)**	**Asphaltenes, Hexane insoluble (wt %)**
0.939	0.906	20.4	2.15	2.81 $\pm$ 0.24	0.040	37	44	16	2.5

Density, TAN, TBN and SARA values obtained from Simon et al. [48]. [a] Karl-Fischer titration was used to determine water content.
Reprinted (adapted) with permission from Simon, S.; Nenningsland, A. L.; Herschbach, E.; Sjöblom, J., "Extraction of Basic Components from Petroleum Crude Oil". Energy & Fuels 2009, 24, 1043-1050. Copyright 2010 American Chemical Society.

Table 2: Available information on chemicals as provided by the vendors. MW: molecular weight. RSN: Relative solubility number, meaning degree of solubility in water for each chemical. Category is an indication of how harmful the chemicals are to the environment (black, red, yellow, green). Chemicals are listed in reference to standards set by the Norwegian classification system (Petroleum Safety Authority Norway) [49].

Chemical #	Category	Type	Chemistry	MW	RSN	Water solubility
1	ND	Drier	Blend	High	6.9	ND
2	Yellow 1	Dropper	Fatty acid alkoxylate ester	High	9.5	Good

ND = Not disclosed by manufacturer.

3.2. Emulsification procedure

15 mL of crude oil was weighed on a balance in a 60 mL cylindrical vial. Then the sample was placed in an oil bath at 65 °C, and a three-bladed propeller was lowered into the sample. The rotor was connected to an Ika® Ultra-Turrax® T 25 disperser. The Ultra-Turrax speed was set to 2000 rpm before continuously injecting 15 mL brine into the sample (50% v/v water cut). This required around 2 minutes to complete. Another 90 seconds were used to mix the brine with the oil before stopping the Ultra-Turrax. A lid was used to close the sample, and then turning it upside down twice to make sure the brine was homogeneously distributed throughout the sample. This was followed up with another 90 seconds of mixing at 2000 rpm.

Following the completion of mixing, demulsifier in xylene or xylene-methanol solution (20 – 100 μL) was pipetted into the 60 mL vial and shaken into the emulsion vertically 50 times. This resulted in chemical dosages of 5-50 ppm of chemical 1, and 80-300 ppm for chemical 2. 2 mL of emulsion was then pipetted into a square glass vial used for parallel plate electric field experiments, comprised of two thick sides (2 mm) and two thin sides (130 μm). The same vial was placed in an NMR for 2 hours of continuous analysis at 65 °C.

3.3. Electric field set-up

A 2 ml emulsion sample was placed in a square vial, of alkali-alkaline earth-silicate glass (or soda lime glass) with reported relative permittivities of k_g = 4.5-9.5 [50]. The crude oil emulsion was placed between two parallel plates of stainless steel (Figure 1a). Glass sides in contact with the aluminum foil are 130 µm in thickness, while the remaining sides are 2 mm thick (Figure 1b). Width and height of the vial is 1 cm and 11 cm, respectively. To ensure proper contact between the glass and steel electrodes, aluminum foil was placed in-between on both sides, and a clamp with rubber insulation was used to keep the electrodes tight. For AC field application a function generator by Agilent Technologies of model DSO-X-2022A was used. It generates maximum 5 volts peak-to-peak, and was connected to a high voltage amplifier by Trek® model 609E-6 that multiplied the output by 1000 volts.

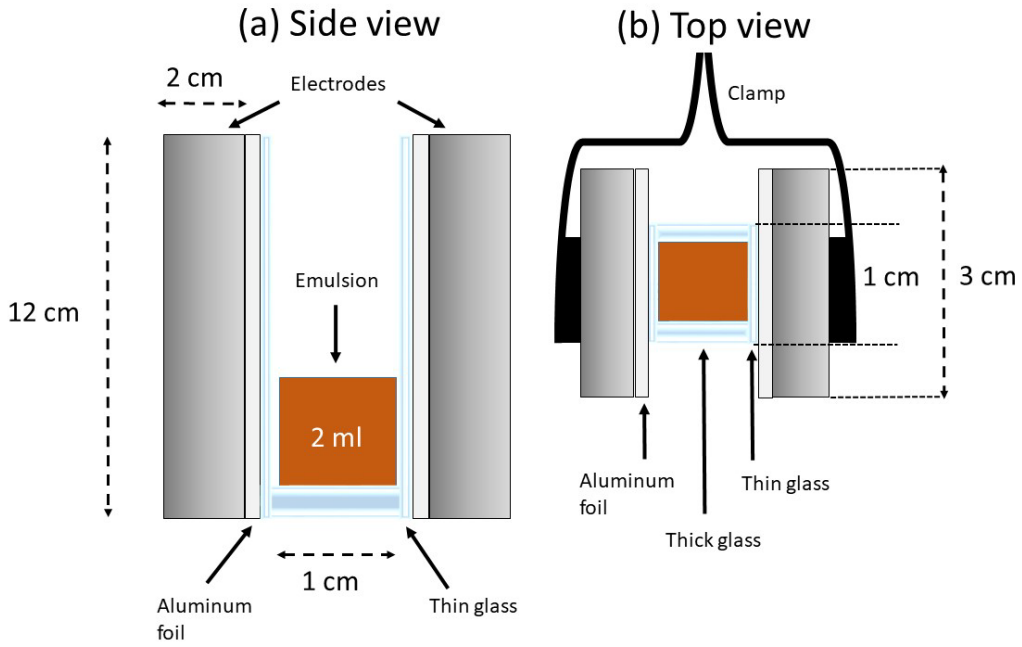

Figure 1: (a) Side view of electric field set-up. (b) Top view of the same set-up. The thin sides of the glass, containing the emulsion, are sandwiched between two stainless steel electrodes with aluminum foil wedged in-between. A clamp is tightened around the electrodes to push the glass walls against the aluminum foil for full contact, which minimizes voltage loss across insulation.

The electric field loss due to the glass cell wall was minimized by using a glass with high dielectric constant (k_g = 9.0) and very small thickness (130 µm). The AC electric field across the emulsion is estimated using the following expression [51];

$$E_e = \frac{\Delta V_o}{\left(h/\varepsilon_e + t/\varepsilon_g\right)\varepsilon_e}, \tag{5}$$

where h and t are emulsion and glass thickness, respectively; while ϵ_e and ϵ_g are electrical permittivities of emulsion and glass, respectively. In an AC field, the electrical permittivity of an emulsion is expressed as [52]: $\varepsilon_e = \varepsilon_e' + j\varepsilon_e''$, where ε_e' and $j\varepsilon_e''$ are real and imaginary permittivities, respectively. Replacing the imaginary term gives: $\varepsilon_e = \varepsilon_e' + j\frac{\sigma_e}{2\pi f \varepsilon_0}$, where σ_e is emulsion conductivity, f is frequency and ε_0 is electrical permittivity for vacuum. Equation 5 is valid for AC fields, although frequency is not very high in the experiments, because the calculated emulsion conductivity, σ_e, is low ($1.3 \cdot 10^{-7}$ S/m), and it is therefore assumed that $\frac{\sigma_e}{2\pi f \varepsilon_0} << \varepsilon_e'$, which gives the simplified expression: $\varepsilon_e \approx \varepsilon_e'$.

Assuming ϵ_e be the permittivity of crude oil, E_e turned out to be 98 % of the externally applied electric field, $E_e = \frac{\Delta V_0}{h}$. The small reduction in the electric field due to the glass can also be ascertained by capacitance measurement assuming the field distribution in the poorly conducting crude oil to be capacitive. Our capacitance measurement for the system, comprising an (emulsion) capacitor inserted in between two (glass) capacitors, suggests that the voltage drop across a glass wall $\Delta V_g = \Delta V_0 \frac{C_g}{C_T}$ is around 0.065 times the externally applied electric potential. Here C_g and C_T are capacitance of glass and total capacitance, respectively. Both estimates suggest a minor reduction in the externally applied field due to the glass walls. Moreover, we tried to minimize the electric field loss by the air gap between glass and the electrode surface by sandwiching a stack of aluminum foil sheets. The glass cell, aluminum stacks and the electrodes were tightly held together by a clamp as shown in Figure 1b. The tender aluminum sheets help in maximizing the glass-electrode contact by squeezing into surface irregularities of a metal electrode and a glass wall.

3.4. Low field NMR for emulsion analysis

To effectively study the demulsification of water, by use of electric field and chemical demulsifiers, from a water-in-oil emulsion, the pulsed magnetic field gradient NMR technique is used. Previous research has validated the PFG NMR method used for the work of this article [53-55]. Anvendt Teknologi AS (Norway) produced the low field NMR instrumentation that has been used for emulsion analysis. The NMR system exhibits a permanent magnetic field strength of 0.5 T (21 MHz), with a maximum magnetic field gradient strength of 3 T/m. With constant air flow to the sample holder, the temperature could be kept at 65 ^{o}C for the duration of the experiment.

3.4.1. NMR sequences

To begin analyzing a crude oil emulsion sample, it is first subjected to a preparation sequence (Figure 1A, Hjartnes et al. [33]), also known as the pulsed field gradient stimulated echo (PFGSTE). This is where the water signal is differentiated from the oil signal. The preparation sequence contains monopolar gradients set to a low value (250 Gauss/cm), and therefore no significant diffusion occurs. Signals from the water and oil may be separated by their respective differences in longditudinal relaxation times (T_1). Since the T_1 of a heavy crude oil is shorter than the T_1 of water, the signal from the oil phase vanishes faster than the water signal. The crude oil signal has to be suppressed by applying a T_1 relaxation time of adequate duration (1 second in these experiments).

There are two characterization sequences: The spin echo sequence (PFGSE) and the CPMG (Carr-Purcell-Meboom-Gill) sequence (Figure 1B and Figure 1C, Hjartnes et al. [33], respectively), and each of these immediately follow the preparation sequence (PFGSTE). When following up the preparation with the PFGSE, the surface-to-volume profile (S/V-profile) can be obtained for the emulsion sample. The surface-volume ratio of a single droplet, is its surface area divided by its volume. This information can be obtained by allowing hydrogens to diffuse and contact droplet boundaries, thereby defining these boundaries, within a short time. This S/V-profile is a relationship between the droplet diameter and the sample position. These S/V measurements emerge from measuring the diffusion coefficient at short observation time (Hjartnes et al. [33], Eqs S.1-S.3, Supp. Info.). Running the CPMG sequence after preparation returns echo attenuations from the water phase, which can be used to calculate a T_2-distribution for the sample. Transverse relaxation, otherwise denoted as T_2, is the time constant for decay towards zero for the transverse spin magnetization. This makes it possible to recover the transverse spin magnetization of hydrogen spins in the water phase, subsequent to pulsed field NMR application. From scaling the T_2 distribution against surface relaxivity, the droplet size distribution (DSD) of the sample is obtained. The Surface relaxivity represents the relaxation strength (which

strongly affects the NMR signal decay rate) by water molecules on droplet surfaces. It is a function of average inverse T_2 and average inverse S/V.

3.4.2. Measured parameters

An experimental data point is completed with minimum 2 parallels, where each parallel is run with the intention to capture different changes in the emulsion over time (Figure 1). The sequences for each parallel are elaborated on below.

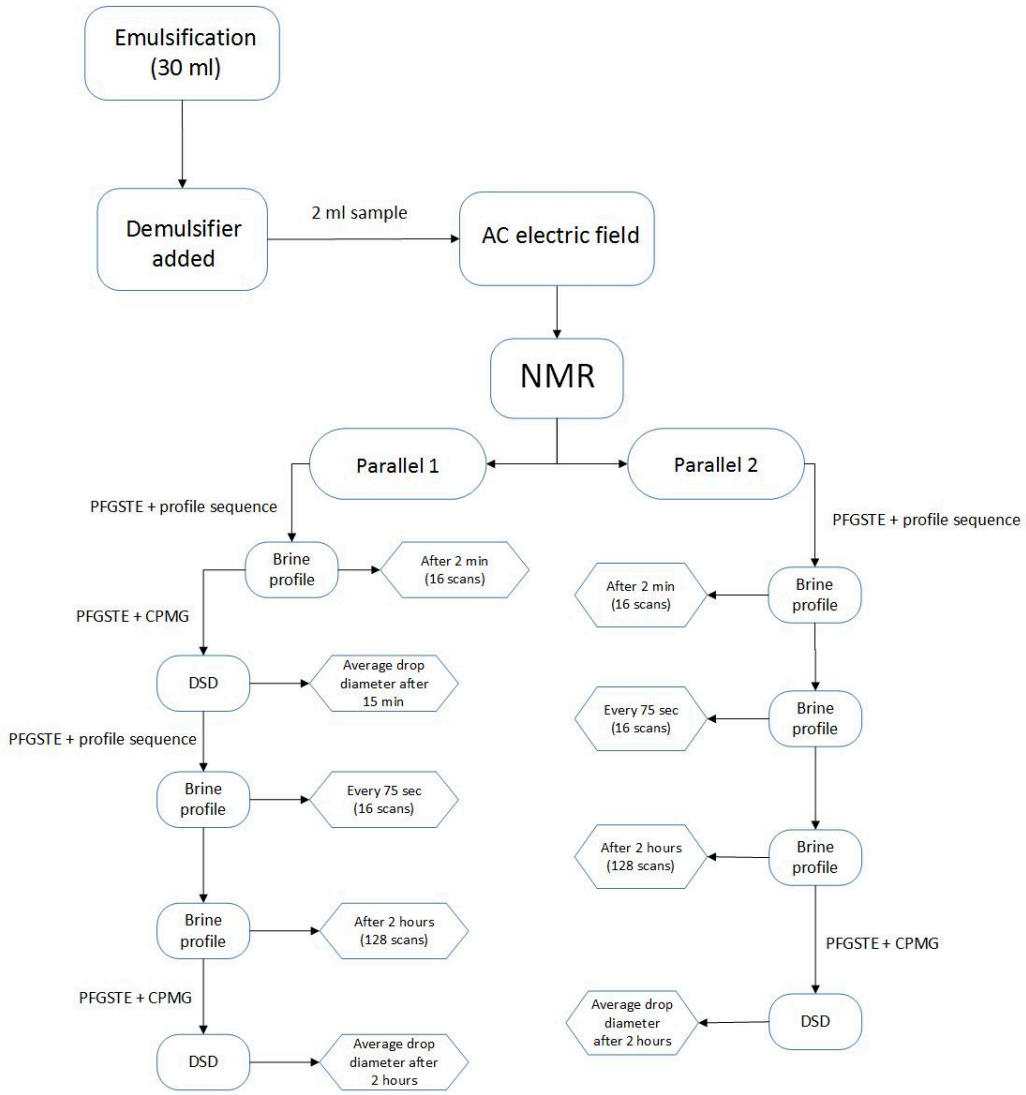

Figure 2: An illustration of the experimental steps taken to treat a crude oil emulsion, from emulsification, to adding demulsifier, applying AC field and quantifying the separation by NMR. In addition, a detailed description is given for the two parallels conducted with the NMR in terms of what is measured and which sequences are used to obtain each measurement.

<u>1st parallel – Droplet size development</u>

When placing a sample inside the NMR, the first measurement is of the droplet size distribution (DSD), which is obtained within the first 15 minutes of separation. These DSDs are useful for knowing which conditions cause slow or fast droplet coalescence, initially. The NMR provides the dimeter of the individual droplets, based on their spherical geometry, and not size of flocs even though droplets may be in contact. Therefore, distinction cannot be made between the droplets that flocculate and the

individual droplets. Consequently, the flocculation phenomena and information on their characteristics is unavailable. Sedimenting droplets eventually accumulate to a free water layer, which is interpreted as a very large droplet that skews the DSD. To make sure that the NMR method only quantifies droplets and not bulk water, a slice selection (see Hjartnes et al. [33] Eqs S.4-S.6, Supporting Information) of the top half oil phase is used. This sliced region will then be representative of only dispersed droplets in the oil phase.

The first DSD measurement is followed by continuous brine profile measurements. To generate a brine profile, the NMR runs the profile SE sequence (Figure S.2 in Supporting Info., Hjartnes et al. [33]), which then constructs a brine profile of the crude oil emulsion every 75 seconds. A brine profile is the measure of the brine content as a function of the sample height (Figure S.2, Supp. Info), which is useful for analysis of droplet sedimentation kinetics. In order to retrieve these profiles in a short amount of time, 16 number of scans are performed, from which the signals are overlapped to create a detailed 2-dimensional picture of the water content. After 2 hours the last brine profile is measured with 128 scans, requiring 9.5 minutes, since the water content in the top oil phase of the emulsion can be extremely low and difficult to quantify. At this point, the emulsion changes are minimal due to slow droplet kinetics which allows for this high number of scans. Once the last profile is obtained, the last droplet size distribution is measured with the same method as the first.

2nd parallel – Free water appearance kinetics

When measuring the DSD, as in the 1st parallel, roughly 15 minutes of emulsion change is lost. For the 2nd parallel, the first droplet size distribution is therefore not measured. Rather, the NMR begins measuring the brine profile straight away (with 16 scans) to capture the droplet kinetics which will be lost when starting with the DSD. After the first brine profile, the NMR continues producing a second and third, and so on until 2 hours has passed. The last brine profile is, similarly to the 1st parallel, measured with 128 scans to capture a more detailed profile as well as water content that may go undetected with only 16 scans. Although the first DSD is skipped, the last DSD is still measured after the last brine profile.

Free water layer

In each brine profile, a clear distinction can be made between bulk water and suspended droplets. Since the crude oil will stick to the glass vial, the water signal from the NMR experiment does not show up as 100%, but rather as approximately 80%. Each data file, containing every brine profile for a particular experiment (≈100 profiles), is run through an isolines program that collects all water contents containing 80% water (with their related sample positions) from each brine profile. The sample positions of 80% water are normalized against the total initial height of the emulsion sample and plotted together in one graph (example shown in Figure S.4a) as normalized sample position against time.

Emulsified water

By assuming 80% water to be bulk, it allows us to calculate the emulsified water content in the top oil phase of the emulsion. This emulsified water content is calculated for the very first brine profile directly after AC field application (after 2 minutes of separation), and again after 2 hours of continuous separation. In order to calculate this emulsified content, the total area (bulk and emulsified water) under the curve of the brine profile is estimated. Then the area under the curve that shows 80% water content (pertaining to bulk water) is estimated. The emulsified water content is then calculated by the following expression:

$$W\%_{\,Total\ area} - W\%_{\,Bulk\ area} = W\%_{\,Emulsified\ area} \quad (6)$$

Residual water

The emulsified water curves are compared to residual water curves, where the water content is read from a single point on the brine profile at 75% of its normalized height (H/H0). This is done for the first (2 min) and the last (2 hours) profiles to cross-check if the trends from the emulsified water estimation are similar to the residual.

Average droplet diameter

In order to get the average droplet diameter in μm, the average surface-volume ratio (m^{-1}) can be converted in the following way:

$$Average\ droplet\ diameter\ (\mu m) = \left(\frac{\overline{S}}{V}\right)^{-1} 6 \cdot 10^6 \quad (7)$$

where the surface-to-volume ratio is an expression that is coupled to the surface relaxivity and the T_2-distribution (see Hjartnes et al. [33] Eq. S.3).

4. RESULTS

4.1. Procedure development

Emulsions of 50% water cut were chosen as water contents of typical crude oils from the Norwegian Continental Shelf can be quite high, sometimes above 50% [56] when reaching the 1st stage of an oil-water separation train. The emulsions were placed inside an electric field (see set-up, Section 3.3). During experimentation at elevated temperatures, the parallel plate set-up with the glass vial was pre-heated inside a heating cabinet at 65 °C. After filling the vial with emulsion, the sample was left in the heating cabinet to temperate for 1 minute before applying the AC fields. All samples were subjected to 30 seconds of AC field, as this was deemed sufficient time for emulsion destabilization during trials. The frequency was kept constant at 1 kHz, close to frequency magnitude typically used in electrocoalescence processes. Field strengths in these experiments were in the range 50 to 700 V/cm RMS. After AC field application, the sample was taken out and placed inside the PFG NMR, and the separation development analyzed for 2 hours in the absence of AC field. This 2 hour separation study was conducted to capture continuing after-effects from the AC field as well as the chemical contribution. Low field strengths were found sufficient enough to separate emulsions with the specific crude oil investigated in this article. The chosen field magnitudes also allows chemical separation effects to emerge, and for their significance in the electrical and chemical interplay to be determined.

It was experimentally observed that, when the electric treatment is performed, the glass vials have limited durability. After a certain amount of experiments (≈ 7-10) a noticeable difference may be seen from the separation efficiency at the initial starting point when the cell was new (see examples Figure S.1a-e, Supporting Info.). Sometimes we can observe cracks in the glass (Figure S.1c, Supp. Info.), and the separation reduction can therefore easily be attributed to this. Other times, there are no visible cracks (Figure S.1b, Supp. Info.) although separation has clearly been weakened (Figure S.1e, Supp. Info.). To achieve reliable measurements, some precautions are therefore taken: 1) Old cells are replaced by new ones regularly. 2) New data are verified against previous data. 3) Two parallels are completed with two different cells. Any error bars that in the results section are based on two or more parallels. Errors stem from calculations of the deviating minimum and maximum values from the

average value. Take note that some error bars in the result section are not observable because they are smaller than the symbol size representing each data point.

4.2. Separation by AC field

Separation of the North Sea heavy crude oil, used for all experiments in this article, proved to be very slow at room temperature due to its high viscosity. Most experiments have therefore been conducted at 65 ^{o}C to reduce the viscosity of the North Sea heavy crude oil (by one order of magnitude) with the aim to match more typical crude oil viscosity values [57] within industrial separators. In addition, chemical 2 (presented in later sections) in this study was specifically designed for performance at temperatures above 60 ^{o}C. Keeping the emulsion above this temperature throughout the entire experiment is challenging as the sampling into the glass vial occurs at room temperature before placing it in the heating cabinet. This may cause the emulsion to be slightly lower than the intended 65 ^{o}C during field application. In addition, the temperature will drop after application of field when the sample is taken out of the heating cabinet (again subjected to room temperature) and carried to the NMR.

4.2.1. AC field only

The performance of emulsion separation of AC field alone will be analyzed and discussed in this section, and used as a baseline in the later sections when comparing efficiencies and mechanisms of chemical demulsifiers in combination with AC field. Figure 2 shows the emulsified water content (calculated with Eq. 6) for increasing voltages (RMS) for an emulsion subjected to AC field after the first 2 minutes, as well as 2 hours later. The 2 minutes is the time it takes from when AC field application ends until the NMR has measured the first brine profile. Any effect seen after 2 min is regarded as a more or less instant result of field application.

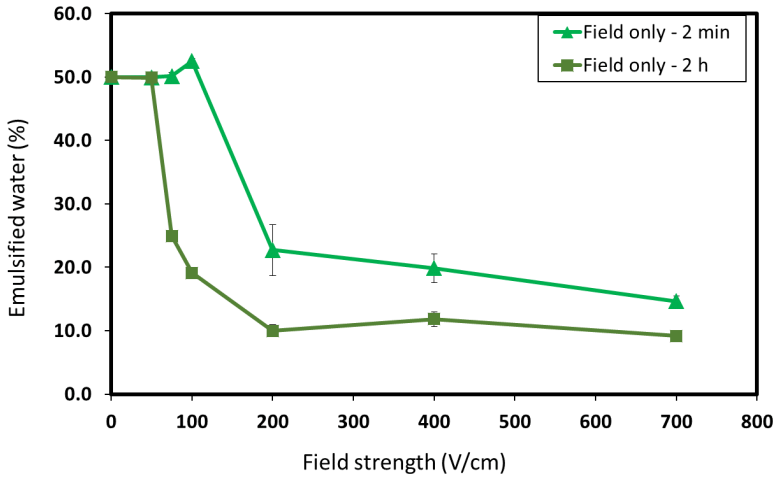

*Figure 3: **Field only.** Emulsified water (%) vs field strength (V/cm) in root mean squared (RMS) values.*

A noticeable difference can be observed from the 2 min to the 2 hour curve, in that the emulsified water content drops over time. This decrease in water content indicates that droplet coalescence and sedimentation, within the emulsion, continues for a while after ended AC field exposure. In the 2 min curve, a minimum field E > 100 V/cm is required for immediate accumulation of a free water layer in the bottom half of the sample. The emulsified water curves correlate well with the trends seen in Figure 3, where the average droplet diameter is shown as a function of field strength. It takes 15 min to quantify the diameter at the beginning of each experiment. It is clear that the initial droplet size (15 min curve) increases in sync with the increasing field strength until 100 V/cm, where the droplets

reach a certain size where they sediment out of the top oil phase. Hence, the existing minimum field strength observed, for initial separation, in Figure 2. The minimum field E ≥ 75 V/cm is required to induce free water separation within the time span of 2 hours. As the field is further increased, larger amounts of water is resolved and the emulsified content decreases until 200 V/cm, at which point no further improvement can be observed in terms of separation. No evolution can be observed in average droplet diameter either, ranging from 100 to 400 V/cm.

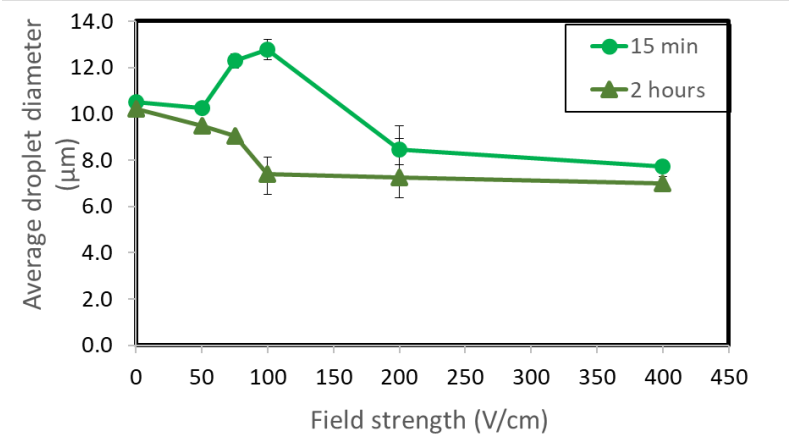

*Figure 4: **Field only.** Average droplet diameter (µm) vs. field strength (V/cm) for an emulsion containing 50% oil phase.*

Figure 4 shows the residual water content (explained in Section 3.5) with increasing field strength The trends reflect that of the emulsified curve from Figure 2 quite well, except that instead of a plateau in the evolution of the water content at E > 200 V/cm, there is still a slight evolution of the residual water content at higher fields. As seen for the emulsified water, a minimum field of E = 75 V/cm is required for release of free water.

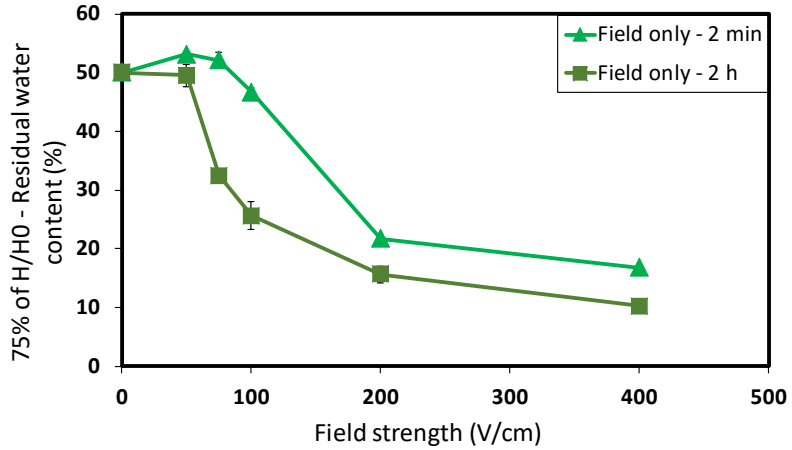

Figure 5: Residual water content at 75% of H_0 vs. field strength (V/cm).

The evolving brine profiles are shown in Figure S.2a-c (Supplementary Info.) for fields 50-100 V/cm. No sedimentation front is observed for any of these fields. Indeed a constant and regular evolution of the WC is seen in the emulsified layer and no sudden drop in the WC appears, specifically at the top of the sample. Since the water cut varies with the position of the emulsified layer, this prevents the calculation of the sedimentation rate. Applying 50 V/cm (Figure S.2a) leads to a slow evolution of the profiles, which indicates adequate electrical forces to coalescence small amounts of droplets. The field is only sufficient to produce a dense packed layer of droplets at the bottom since the water content does not exceed 80% for the last profile. Increasing the field to 75 V/cm (Figure S.2b) coalesces

droplets faster, seen from the 0 min profile already showing signs of sedimentation. A free water layer is collected after some time and a water cut gradient becomes more apparent from bottom to top of the sample. Droplets are generally smaller dat the top, and these seem to coalesce faster than the larger ones located further down. At 100 V/cm (Figure 2c), the 0 min profile displays droplet sedimentation, indicated by the peak. Another peak is located right above the halfway mark of the sample, which could mean that some droplets are in a dense packed layer formation over the water-oil interface. This peak smooths out over time by drop-drop and drop-interface coalescence. The gradient of decreasing water content from halfway to the top is even sharper than for 75 V/cm.

4.2.2. AC field and chemical: Influence of electric potential

This section is deals with the investigation into how emulsions in an external AC field is affected by the addition of a chemical demulsifier. These chemicals are from two different vendors (NalcoChampion and Nouryon), of different water solubility (in ref. RSN in Table 2) and molecular composition. Chemical 1 is used at a fixed concentration of 10 ppm throughout all experiments where the electric potential is investigated. This concentration was found to be optimal in a previous investigation [33] of this chemical in absence of electric field, although the emulsification conditions were different. Chemical 2 is varied between 120-300 ppm as the optimum concentration from the previous study was within this range.

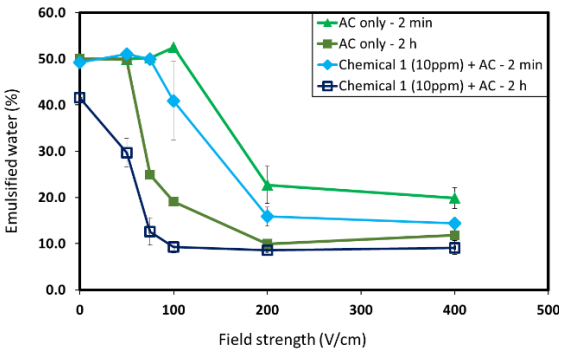

*Figure 5a: **Chemical 1 (10 ppm)** and AC field. Emulsified water (%) vs. field strength (V/cm).*

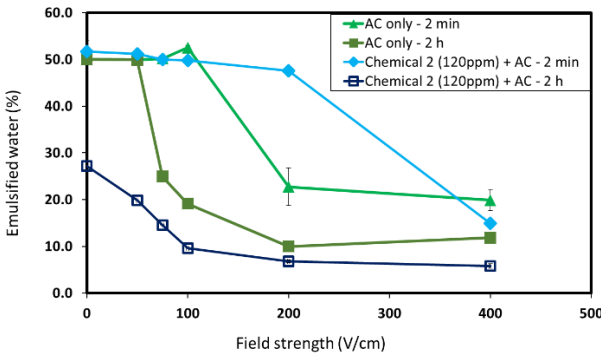

*Figure 5b: **Chemical 2 (120 ppm)** and AC field. Emulsified water (%) vs. field strength (V/cm).*

Figure 5 shows emulsified water with increasing field strength for both chemical 1 (Fig. 5a) and chemical 2 (Fig. 5b-c). In each plot, the AC field curves (light and dark green) from Section 4.2.1 are used as baselines to observe possible synergetic effects for each chemical together with the AC field. In Figure 5a, the 2 min curve of chemical 1 + AC field (light blue) follows a near identical trend to the 2 min AC field only (light green). This trend signifies that separation is controlled by the field in the early stage, and that chemical 1 has yet to take effect. Therefore the minimum voltage required for a significant reduction of emulsified water is still E > 100 V/cm. After 2 hours, a larger difference can be seen between field only (dark green) and chemical 1 + field (dark blue). A minimum field of 50 V/cm for appearance of free water has been reduced to 0 V/cm when chemical 1 is added. Furthermore, the curve in the range of 50 – 100 V/cm for chemical and field lies beneath the field only curve, having improved the final water separation over the course of 2 hours. Synergy between chemical demulsification and electrocoalescence is therefore visible in the field range 50 – 100 V/cm. As E ≥ 200 V/cm, the field dominates the separation, and no visible effect is shown from chemical 1.

There is an existing sedimentation front for chemical 1 in the range 50 – 100 V/cm of synergy (see Figure S.3a-b, Supporting Information). A clear sedimentation front is visible at 50-75 V/cm, while droplets are quite large at 100 V/cm which leaves a very small window for characterization of sedimentation. When studying the progression of the brine profiles in the range of 50 – 100 V/cm, it can be noted that the water content diminishes most rapidly from the very top 1/5th of the emulsion.

However the reducing front concerns only part of the droplets. There are still residual droplets present at the top of the sample. Perhaps these exist due to their size keeping them suspended, which is especially noticeable at 75 V/cm of Figure 6a (15 min), and unable to coalesce upon drop-drop collision while large droplets have settled out. With decreasing water content in the upper half at 100 V/cm (Figure S.3c), a peak becomes visible above the water-oil interface. This is possibly a dense packed droplet layer unable to coalesce with each other and the interface. One reason could be that the demulsifier does not necessarily remove the entire layer of indigenous crude oil components, but only breaches part of it to allow droplets to coalesce and sediment closer to the interface without coalescing with it. For chemical 2 there were no observed sedimentation fronts (Figure S.5a-c, Supp. Info.). The reason behind this difference is currently not known. The profiles for chemical 2 have less sharp water gradients than for an emulsion treated with chemical 1. This could mean that the emulsion dehydration is more evenly distributed with chemical 2, and not targeted towards smaller droplets as seen for chemical 1.

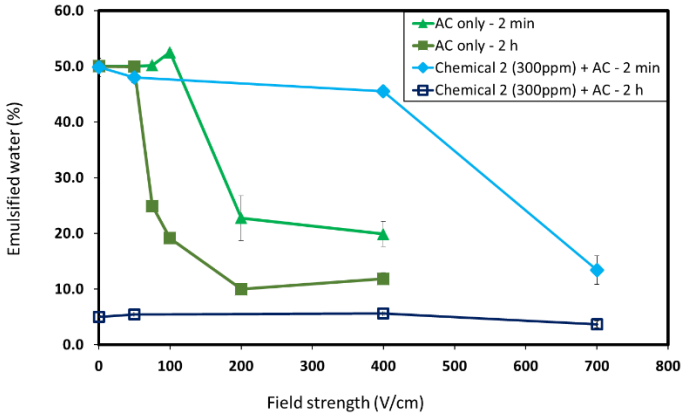

Figure 5c: **Chemical 2 (300 ppm)** and AC field. Emulsified water (%) vs. field strength (V/cm).

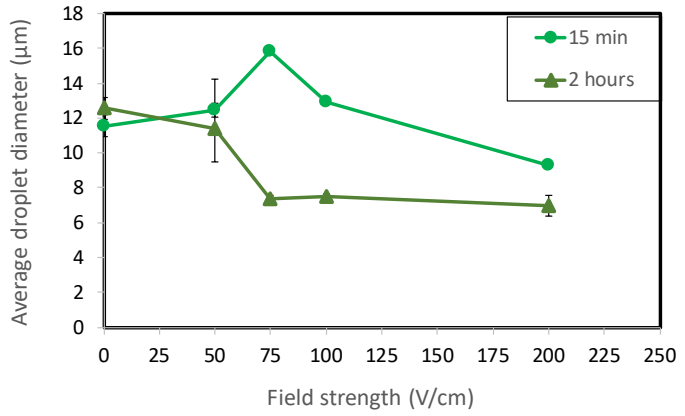

Figure 6a: Average droplet diameter (µm) vs. field strength (V/cm). ***Chemical 1 (10 ppm)***

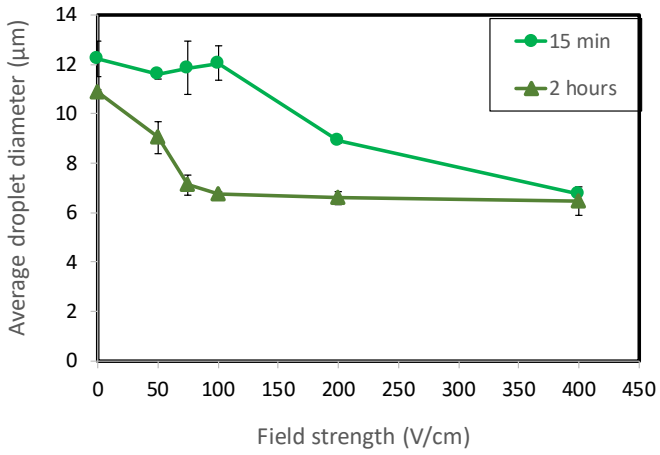

Figure 6b: Average droplet diameter (µm) vs. field strength (V/cm). ***Chemical 2 (120 ppm)***

Experimental sedimentation rates are estimated by creating iso-volumetric curves (see Figure S.4a-b), Supp. Inf.). The rates are then estimated by tracking the initial linear trend in a selected iso-volumetric curve of 35% water content (see Hjartnes et al. [33] Figure S.5, Supp. Info.). This curve constitutes all brine profiles for a specific system of a given water content. A slope is calculated from the linear trend line (black dotted lines in Fig. S.4a-b), which is multiplied by the sample height to obtain the sedimentation rate.

Comparison can be drawn between experimental sedimentation rates and the theoretical rates. Since the Stokes' equation, for describing drag, is mainly valid in cases where no slip occurs between the settling droplet and the surrounding medium, a correction factor was been added by Dickinson and Stainsby [58]. However, when the viscosity of the droplet is significantly less than the viscosity of the continuous fluid, the settling rate is 1.5 times faster than the original Stokes' equation. So even with the correction factor, the droplet velocities would still be in the same order of magnitude, and we will therefore refer to the original Stokes' equation for calculating the settling velocity [58]:

$$u = \frac{d^2 g|\Delta\rho|}{18\mu}, \tag{8}$$

where $\Delta\rho$ is the density difference between oil and water, g is the gravitational constant, d is the droplet diameter and µ is the viscosity of the oil.

The calculated Stokes' sedimentation rates are listed together with the experimental sedimentation rates in Table 3. The ratio between experimental and Stokes shows that the experimental rates are generally larger than the theoretical ones. A similar phenomenon was seen in a previous study (chemical demulsification only) [33], where the faster experimental sedimentation was attributed to the possibility of flocculating droplets, and the fact that the emulsion is polydisperse rather than monodisperse (as assumed for the Stokes' equation).

Table 3: Chemical 1 and AC field. Sedimentation rates (mm/min) for the applied AC fields in which the synergetic effect between chemical 1 and the field was observed. Comparison between experimental sedimentation rate and sedimentation rates calculated from Stokes' equation, using initial average droplet radiuses.

Field (V/cm)	u_{exp} (mm/min)	u_{stokes} (mm/min)	$\frac{u_{exp}}{u_{stokes}}$
50	0.04 ± 0.01	0.02	1.63
75	0.12	0.04	3.01
100	2.01	0.03	77.25

The largest discrepancy between experimental and theoretical values can be seen at 100 V/cm. This difference could in part have been caused by the fact that the diffusion measurements to obtain the DSD takes roughly 15 minutes, at which point the rapid changes in the droplet diameters could already have taken place. If the sedimentation of droplets in the emulsion happen at a very rapid pace, which is the case according to the experimental rate at 100 V/cm, the NMR measurements are not conducted quickly enough to reflect the real initial average diameter of droplets. At 200 V/cm and above, the changes occur so quickly that no sedimentation rate could be calculated. On another note, if droplet sedimentation is predominantly controlled by flocculation, this phenomenon would not be identifiable through NMR measurements. Therefore, flocculation might be yet another reason why differences of initial average droplet diameters are not more significant.

More information can be gathered about the extent of separation improvement, and the synergistic effect between chemical 1 and AC field from the curves that represent sedimentation and free water layer positions in Figure S.4a-b (Supplementary Information). The sedimentation plots follow points in the sample containing 35% water content, while the free water plots follow points containing 80% water content (essentially free water). Each plot also has a number of curves, including both sedimentation position and free water layer height of 1) field only, 2) chemical only and 3) chemical + field. Two conditions are selected from the electric potential range (75 and 100 V/cm) where the most drastic changes occur.

Free water layer height comparisons (after 2 hours of separation) are made in Figure S.7a, between AC only, chemical 1 and chemical 2. Differences in the free water resolved occur most noticeably at 50 V/cm, where the field is weak enough to leave partial separation to chemical effects. At E ≥ 100 V/cm, no distinction can be made in the final separation when using either chemical at their respective concentrations. Free water appearance times are shown in Figure S.8a (Supp. Info.) with increasing concentrations for AC only, as well as chemical 1 and 2. It is most noticeable how chemical 1 and 2 both drastically reduce the appearance time from AC only at 50 V/cm. Past this field, the differences gradually vanish as the AC field effects become more a more prominent factor in the separation process. This can be seen from Figure S.8b, where the area of interest has been enhanced from Figure S.8a. At 100 V/cm, chemical 1 + AC is the only curve that displays immediate free water appearance (seen more clearly from Fig. S.8b). As the field increases to 200 V/cm, AC field only also resolves an immediate free water layer. For chemical 2, this free water layer does not appear until 400 V/cm, as was also observed from the emulsified water curves (Figure 5b).

Following the (light green) free water curve of chemical 1 + 75 V/cm (Figure S.4a, Supp. Info.), the initial rate of free water formation is identical to that of 75 V/cm field only (teal). This overlap indicates that the early separation stage is dominated by the AC field effects. At a certain point, however, the free water layer height of chemical 1 + field surpasses that of field only, meaning that the chemical is taking effect and aiding the water resolution. The same can be said for their respective sedimentation curves, where the initial sedimentation overlaps before a gradual distinction emerges, as the curve of chemical 1 + field (orange) overtakes field only (teal). In Figure S.4b (Supp. Inf.), the free water layer

of chemical 1 + 100 V/cm (green) shows a greater gap from 100 V/cm field only (teal). The separation is no longer controlled by the field at the initial stage, and the added chemical contributes to an immediate, thin free water layer that is not observable with the use of field only. The sedimentation occurs much faster in the system subjected to chemical 1 + 100 V/cm (orange) in comparison to 100 V/cm field only (red), as more droplets coalesce and grow larger after field application in the presence of chemical 1. This droplet increase can be seen by comparing 15 min curves in Figure 6a (chemical 1 + 75 V/cm) and Figure 3 (75 V/cm only). After 2 hours of continuous separation (Figure 5a), the emulsified content of chemical 1 + field (dark blue) has significantly dropped compared to after 2 min (light blue). Direct correlation can be made between these curves and the evolution of the average droplet diameter (Figure 6a), where the droplet size has become visibly smaller as all the largest droplets, resulting from coalescence, have fallen out of the top oil phase. No further evolution of size occurs past 75 V/cm, at which point the emulsified content of chemical 1 + field in Figure 5a is close to the plateau.

Figure 5b contains the same baselines of AC only (green curves) together with the performance of chemical 2 in combination with AC field (blue curves). The minimum field required for an immediate (2 min) release of free water seems to increase when subjecting the emulsion to chemical 2 in addition to AC field, as free water is observed at E > 200 V/cm compared to E > 100 V/cm for field only. It is apparent that the chemical initially retards the coalescence of droplets at 200 V/cm in comparison to the surface active counterparts of the crude oil. Above 200 V/cm, the field is so strong that it overtakes the chemical effects, and the emulsified content coincides with that of field only at 2 min. At fields below 200 V/cm, the final emulsion separation efficiency after 2 hours is enhanced by chemical 2, also seen from Figure S.6a (Supporting Information). The free water curve of field only at 75 V/cm (teal) is far out-performed by chemical 2 + 75 V/cm (green), both in terms of the rapid changes in the early stage and the final amount of separation.

The differences of field with and without chemical 2 are reduced at 100 V/cm (Figure S.6b, Supp. Inf.), where the initial rate of free water layer for field only (teal) overlaps with that of chemical 2 + 100 V/cm (green), and the separation is dominated by the AC field effects. The chemical continues increasing the thickness of the water layer onwards from the point where the AC field reaches its maximum potential. Emulsion separation, when using chemical 2, has not exhibited any sedimentation front (Figure S.5) as was seen for chemical 1 (Figure S.3). Because of this lack of a linear relationship between sample position and time, no sedimentation rate could be estimated. Even if chemical 2 has no sedimentation front after electrical treatment (Figure S.5, Supp. Info.), we have considered the 35% iso-volumetric profile as an indicator of sedimentation of droplets. For this sedimentation curve (iso-volumetric profile), chemical 2 + 100 V/cm (orange) in Figure S.6b leads to more droplets accumulating to free water than 100 V/cm only (red), although the performance when adding the chemical is the not much different from 75 V/cm with chemical. Looking at the initial average droplet size diameter after 15 min (Figure 6b), the size remains unchanged between 0 – 100 V/cm when using chemical 2, which could indicate that droplets coalesce and sediment so fast that it is not captured by the NMR measurements. It could also be a possible sign of flocculating droplets, as the NMR is unable to distinguish between isolated and contacting droplets.

The concentration of chemical 2 has been increased to 300 ppm together with an AC field in Figure 5c. After 2 hours, immediate separation occurs when exceeding fields of E > 100 V/cm for AC only, while chemical 2 (300 ppm) with AC requires E > 400 V/cm. This concentration thereby exhibits the same phenomenon of retarding initial droplet coalescence as observed at 120 ppm, only this time the delay is further amplified. The higher concentration of chemical 2 displays the trait of an over-dosage in the early separation stage. However, the separation is overall improved after the initial stage. Increasing the field with the addition of 300 ppm proves to be redundant as it unveils no further improvement for the final separation (dark blue). The chemical has become the dominant factor (Figure 5c). An important point to note in regards to the kinetics of each concentration, is the fact that

at 120 ppm the free water layer gradually rises to 60% of its maximum thickness over 2 hours. While the free water layer at 300 ppm (not presented) reaches 80-90% of its potential thickness within 10 minutes.

Residual water contents (Figure 7a-b) for chemical 1 and 2 both follow similar trends as the emulsified water curves (Figure 5a-b). It can be observed that the residual water content may be reduced at all fields when combining electric field with chemical demulsifiers. It can also be noticed that the residual water cut cannot be reduced below 5-10% even at the highest field tested, 400 V/cm. The reason why the residual water content does not fall below this value is unknown. A possible explanation could be that some droplets are stuck on the walls due to the size of the cell and the water wetting properties of the glass.

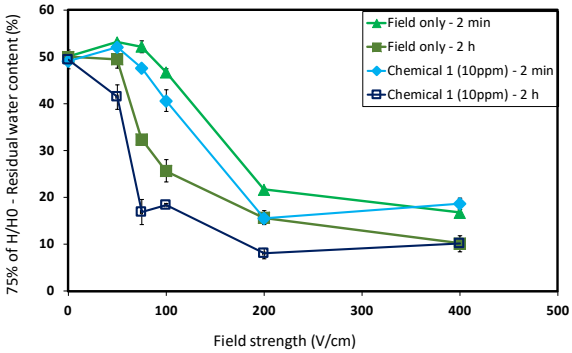

*Figure 7a: **Chemical 1 (10 ppm)** and AC field. Residual water (%) vs. field strength (V/cm).*

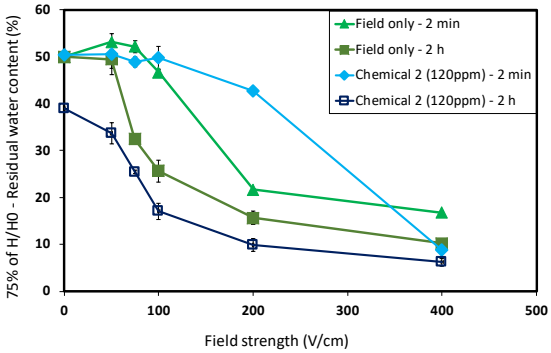

*Figure 7b: **Chemical 2 (120 ppm)** and AC field. Residual water (%) vs. field strength (V/cm).*

Electrical capillary number may also explain the previously encountered emulsified thresholds seen in Figures 4, 5 and 7. The balance between electric stresses and interfacial tension determines the shape of a drop under an electric field. The electrical capillary number $Ca_E = \frac{k_m \varepsilon_0 a E_0^2}{\gamma}$ governs the shape and stability of the drop. At a constant Ca_E the drop holds a stable shape. However, when Ca_E is increased above a critical value - called critical electrical capillary number - the drop loses its equilibrium shape and breaks into a number of drops depending on mode of the breakup (Torza et al. 1971 [59], Manga & Stone 1999 [60]). In an emulsion under electric field, the enlarged drops exceed the critical electrical capillary number and undergo a breakup (Mhatre & Thaokar 2014 [61]). The phenomenon introduces tiny droplets in the emulsion and reduces its average droplet size, especially when the applied field is very strong or the interfacial tension is very low. In crude oil emulsions, the water-oil interface is covered with a variety of surface active components indigenous to the oil, which alters its interfacial properties. The low interfacial tension makes the droplets susceptible to instability under strong electric fields. Therefore maintaining the electrical capillary number below the critical by controlling the operating electric field with the progress in the separation helps to attain a desired water content and to prevent further homogenization of the emulsion.

4.2.3. AC field and chemical: Influence of concentration

The effect of the chemical concentration has been investigated in this section, while the electric potential is kept constant at a value of 50 V/cm. This field was chosen because it is low enough to not dominate the separation process so that effects of the added chemical become more prominent, based on previous observations from Figure 5a-b. With a field as low as this, synergistic effects may

be visible even at high concentrations. Three chemicals have been selected for comparison of their contributions towards water separation: Chemicals 1 and 2 (Table 2).

Concentration effects on emulsified water and free water appearance kinetics

In Figure 8a, the effect of chemical 1 has been plotted both without (green) and with (blue) AC field, 2 min after emulsion treatment and 2 hours later. Chemical 1 requires at least 10 ppm for a free water layer to appear in absence of field, and a certain amount of the emulsion is separated down to approximately 30% final emulsified water content before reaching a plateau between 20-50 ppm. In the presence of a low field (dark blue), all concentrations from 5 ppm and higher resolves additional water after 2 hours, and a synergy is visible within the entire concentration range. It is interesting to note that the concentration of chemical 1 lowers final emulsified content up to 20 ppm before improvement stagnates when used in absence of field, but together with a low field it efficiently enhances separation when the dosage is increased past 20 ppm. Figure S.9a-b (Supplementary Information) shows the free water layer improvement for 20-50 ppm, both with (green) and without (blue) fields. We can see that even though the chemical alone (blue curve in Fig. S.9a-b) does not provide significant free water layer increase, the addition of the applied 50 V/cm significantly speeds up sedimentation (orange curves in Fig. S.9a-b) as well as the final separation (green curves in Fig. S.9a-b). The average measured droplet diameter (Figure S.12a, Supp. Inf.), from 15 min to 2 hours, shows that a small decrease in size can be observed at 20 ppm of chemical 1, while a larger decrease in the size occurs for 50 ppm, meaning droplet coalescence and sedimentation has increased between these concentrations.

As previously mentioned, there is an existing sedimentation front when using chemical 1, both with and without AC field. The sedimentation curve can be observed (orange) in Figure S.9a-b, where the black dotted line represents the trend line of which the slope is calculated that gives the sedimentation rates. Table 4 list the calculated experimental and theoretical sedimentation rates. It is clear that the increasing dosages of chemical 1 leads to higher sedimentation rates, and that the additional field further speeds up the droplet velocities. The cause for this could be attributed to either higher drop-drop coalescence frequency or that the chemical more readily makes way for droplet flocculation by replacing parts of the viscoelastic layer that covers the interface. The increasing concentrations also widens the difference between experimental and theoretical values. This means that coalescence and sedimentation of droplets, by means of increasing concentration of demulsifier and raise in electric field strength, too rapid for DSD measurements (15 min) to capture the average droplet diameter. These measurements are likely occurring after a significant portion of the biggest droplets have moved below the slice region where it can not be detected by NMR anymore.

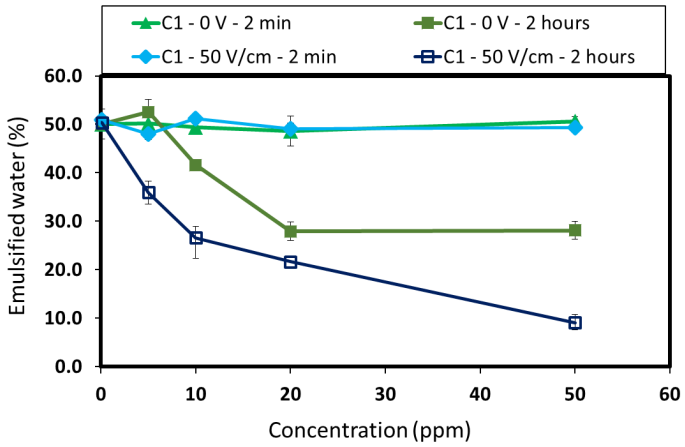

*Figure 8a: Emulsifier water (%) vs. concentration (ppm) of **chemical 1,** with 50 V/cm and without AC field.*

Table 4: Sedimentation rates for chemical 1 only, as well as for chemical 1 + 50 V/cm. Comparison is made between the experimental droplet velocity and the theoretical Stokes velocity (Eq. 8).

Concentration (ppm)	$\mathbf{u_{exp}}$ **(mm/min)**	$\mathbf{u_{stokes}}$ **(mm/min)**	$\frac{u_{exp}}{u_{stokes}}$
Chemical 1			
10	0.018	0.024	0.8
20	0.036	0.021	1.8
50	0.041 ± 0.01	0.027	1.5
Chemical 1 + 50 V/cm			
10	0.040 ± 0.01	0.023	1.6
20	0.065	0.022	2.9
50	0.260	0.029	8.9

Emulsified water content in Figure 8a shows a greater separation efficiency when compared to the residual water content in Figure S.11a (Supp. Info.). This differences is especially apparent when comparing the use of chemical 1 in the absence of field, which indicates that the chemical effectiveness varies depending on the sample position. This can in turn be related to specific droplet sizes being targeted by the chemical. It was similarly seen that the brine profiles of chemical 1 reduced faster from the top 1/5th of the emulsion, which supports the idea of its effectiveness towards the smallest droplets.

The emulsified water content is plotted for chemical 2 in Figure 8b, showing the effects of increasing concentration from the chemical alone (green), as well as for the chemical with a low field (blue). There is a small improvement of water separation after 2 hours when combining chemical and field (dark blue). A visible synergy is present through all concentrations used. This chemical dominates more of the separation process at a low field compared to chemical 1, although a lower dosage is also required for chemical 1 in general to reach the same efficiencies. From 80 ppm to 160 ppm, the free water layer height (Figure S.10a-b, Supp. Inf.) forms faster together with a low field (green curves). At 160 ppm, the chemical alone (blue) is able to reach a very similar final amount of resolved water as for chemical 2 + field (green) after 2 hours. Even though no sedimentation fronts are present, the 35% curves (orange) indicates the speed of droplet sedimentation. We can see that there is a large improvement of increasing the dosage from 80 ppm (Fig. S.10a) to 160 ppm (Fig. S.10b), and that the 50 V/cm field adds a drastic improvement to the sedimentation speed at 160 ppm. At 300 ppm (not shown), the chemical concentration is so high that no difference can be made between chemical effects alone and chemical with field. A larger increase is also seen in the droplet size after 15 min in Figure S.12b (Supp. Info.). At this concentration, sedimentation and free water layer curves also reflect the same separation speeds as for the chemical alone.

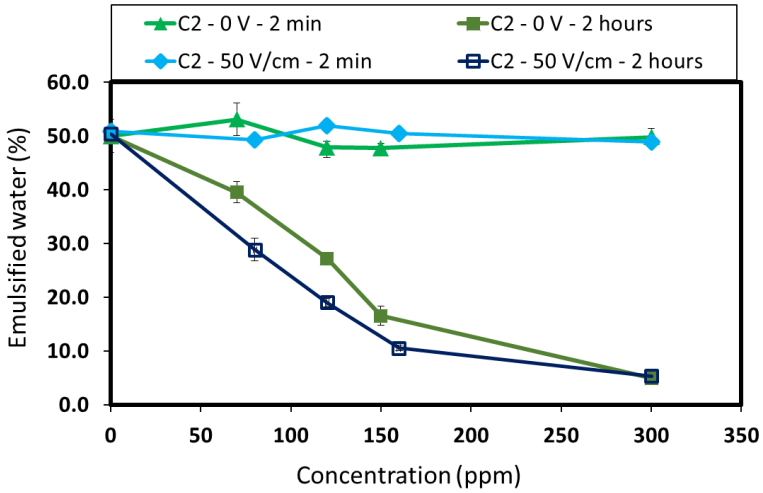

*Figure 8b: Emulsifier water (%) vs. concentration (ppm) of **chemical 2,** with 50 V/cm and without AC field.*

Residual water content in Figure S.11b seems to follow a similar trend to that of emulsified water in Figure 8b, which indicates that the droplet reduction from the emulsion, when using chemical 2, is uniformly distributed. This chemical is therefore effective in targeting large droplets, as opposed to chemical 2.

5. DISCUSSION AND CONCLUSION

A next generation low field NMR procedure developed in a preceding study (Hjartnes et al. [33]), and utilized for analysis of chemical demulsification performance in crude oil emulsions, was extended within this article to comprise demulsification in combination with external electric fields. Several parameters that are known to influence chemical and electrical demulsification processes were investigated. Namely, effects from field strength, demulsifier composition and chemical concentration.

In AC fields only, the crude emulsion showed immediate (2 min) response to E > 100 V/cm, and an improved overall separation (2 hours) for E > 50 V/cm. Synergy exists for both chemical 1 and 2 with AC fields, but only in a range low enough where field effects are not dominant (50-100 V/cm). The immediate effect on the emulsion from AC with chemical 1 follows the same trend as AC only, which indicates AC field dominance in early separation stages. This AC field control was not experienced when using chemical 2, as initial separation was slowed down for the same field strengths. Chemicals 1 and 2 aided further separation for AC fields. Chemical 1 leads to a significant increase in initial droplet size in area of synergy (75-100 V/cm).

The fixed dosage (10 ppm) used for chemical 1 did not fare particularly well in demulsifying the crude emulsions of larger droplet size (≈12 μm) unaccompanied by electric field (Table 5). Performance drastically increased when using low concentrations (10-50 ppm) of chemical 1 in combination with low AC fields (50-100 V/cm). The chemical seems to work well when dealing with small droplets (≈6 μm), which was particularly apparent the previous study, shown in Table 5. In conjunction with an AC field, which coalesces large droplets very well, the emulsion separation improves past basic AC field capabilities when combined with both chemicals. Above a given field strength, the AC field dominates the separation and the effect of chemical demulsifiers are barely visible.

Chemical 2, as a demulsifying agent, separated crude oil emulsions successfully by itself, and even though higher concentrations were used no separation stagnation was experienced. As Table 5 shows, chemical 2, in the absence of field, performed better in a system of larger droplets (≈12 μm) compared to the system with smaller droplets (≈6 μm) where concentrations are also significantly higher. Like the first demulsifier, chemical 2 effectively promoted free water when combined with low AC fields past the ability of the field itself. At higher AC fields (200-400 V/cm), an overdosing effect began to take place that would detriment the initial drop-drop coalescence rate. This droplet retardation effect became enhanced by increasing chemical 2's concentration. Over-dosing effects were not observed when using chemical 1, but no distinction could be made in separation efficiency of using AC field only or chemical 1 with AC in E ≥ 200 V/cm.

There is a distinction in the fundamental mechanisms with which chemical 1 and 2 reduce emulsified water, which is apparent from the brine profile evolution. Droplet sedimentation progresses in a sedimentation front throughout the emulsion when treated with chemical 1, which is not the case for chemical 2 as it presents a uniform decrease in the emulsified layer. Sedimentation rates were calculated for chemical 1 with and without AC fields. Experimental rates show increased sedimentation rates when field strength increases. Higher sedimentation rates were calculated for experimental than theoretical Stokes' values. From an inter-drop mechanistic standpoint, we have mentioned flocculating droplets to account for this Stokes deviation, similarly reported by Frising [62] and Barrabino [63].

Table 5: Comparisons between achieved separation efficiency of crude oil emulsions, in the absence of electric field, using chemical 1 and 2 in systems of different average droplet diameter. One system is presented in this article (≈ 12 μm) and the other in Hjartnes et al. [33] (≈ 6 μm).

Average initial droplet diameter			
≈ 12 μm		≈ 6 μm	
Chemical 1			
Concentration (ppm)	**Emulsified water (%)**	**Concentration (ppm)**	**Emulsified water (%)**
0	50.0	0	50.0
5	49.8 ± 2.7	5	26.9 ± 0.8
10	41.6 ± 0.0	10	13.9 ± 0.5
20	29.8 ± 1.9	20	16.4 ± 1.9
50	26.2 ± 1.9	50	10.7 ± 0.7
Chemical 2			
Concentration (ppm)	**Emulsified water (%)**	**Concentration (ppm)**	**Emulsified water (%)**
0	50.0	0	50.0
80	37.6 ± 2.0	214	49.5 ± 0.4
120	27.2 ± 0.3	300	21.9 ± 0.6
160	14.8 ± 2.0	420	20.1 ± 0.4
300	5.0 ± 0.3	662	17.7 ± 1.5

Grimes [64] compared a mathematical model for batch gravity separation by demulsifier with experimental data obtained by low field NMR. He found the degree of poly-dispersity in the emulsion to be the most central factor for rate of droplet binary coalescence and sedimentation. Similar model application studies as Grimes' on our data would be useful for a more robust conclusion in terms of which mechanisms the chemicals operate with to enhance emulsion dehydration. Discrepancies could also be attributed to faulty assumptions about monodisperse emulsion, when in fact it is more polydisperse. It could also be due to flocculation, which Stokes does not account for. More importantly, the initial evolution of the DSD was perhaps too rapid for detection by the measurements.

In the early separation stages, increasing concentrations of chemical 2 seems to momentarily enhance the strength of the interfacial film surrounding the droplets, since higher concentration leads to higher required fields for immediate free water appearance. A phenomenon like this would suggest that the rupturing of the interfacial film slows down. Due to field effects controlling the early separation in presence of chemical 1, it suggests that the chemical has not penetrated the interface or replaced enough indigenous crude components to weaken the viscoelastic layer significantly. As time

progresses, a larger surface coverage is achieved, aiding further drop-drop collision by Brownian motion.

In all emulsified profiles, whether emulsions treated with or without chemicals in AC field, a water content limit is reached. This threshold could possibly be attributed to droplet adherence on the water wetting glass walls. Another point that was raised concerned the balance between electric stresses and droplet interfacial tension of droplets. Droplet enlargement by electric field may lead to the critical electrical capillary number becoming exceeded, resulting in droplet destabilization and subsequent break-up.

Results obtained for this chemical demulsification and electrocoalescence study should be compared with similar studies performed on other types of crude oils to determine the universality of the conclusions drawn.

DECLARATION OF COMPETING INTEREST

The authors declare that they have no conflict of interest.

ACKNOWLEDGEMENTS

The authors thank the JIP Electrocoalesence Consortium, New Strategy for Separation of Complex Water-in-Crude Oil Emulsions: From Bench to Large Scale Separation (NFR PETROMAKS), consisting of Ugelstad Laboratory (NTNU, Norway), University of Alberta (Canada), Swiss Federal Institute of Technology in Zurich (Switzerland), Institutt for Energiteknikk (Norway) and funded by Norwegian Research Council (Grant No. 255174) and the following industrial sponsors: Anvendt Teknologi AS, Equinor, NalcoChampion, Nouryon, and Sulzer.

6. REFERENCES

1. Sjöblom, J.; Johnsen, E. E.; Westvik, A.; Ese, M.-H.; Djuve, J.; Auflem, I. H.; Kallevik, H., Demulsifiers in The Oil Industry. In *Encyclopedic Handbook of Emulsion Technology*, Sjöblom, J., Ed. CRC Press Boca Raton 2001; Vol. 1st Edition, pp 595-619.
2. Less, S.; Hannisdal, A.; Sjöblom, J., Dehydration Efficiency of Water-in-Crude Oil Emulsions in Alternating Current Electrical Fields. *J. Dispersion Sci. Technol.* **2010,** 31, (3), 265-272.
3. Sjöblom, J.; Aske, N.; Harald Auflem, I.; Brandal, Ø.; Erik Havre, T.; Sæther, Ø.; Westvik, A.; Eng Johnsen, E.; Kallevik, H., Our current understanding of water-in-crude oil emulsions.: Recent characterization techniques and high pressure performance. *Adv. Colloid Interface Sci.* **2003,** 100-102, 399-473.
4. McLean, J. D.; Kilpatrick, P. K., Effects of Asphaltene Solvency on Stability of Water-in-Crude-Oil Emulsions. *J. Colloid Interface Sci.* **1997,** 189, (2), 242-253.
5. Mhatre, S.; Vivacqua, V.; Ghadiri, M.; Abdullah, A. M.; Al-Marri, M. J.; Hassanpour, A.; Hewakandamby, B.; Azzopardi, B.; Kermani, B., Electrostatic phase separation: A review. *Chem. Eng. Res. Des.* **2015,** 96, 177-195.
6. Eow, J. S.; Ghadiri, M., Electrostatic enhancement of coalescence of water droplets in oil: a review of the technology. *Chem. Eng. J.* **2002,** 85, (2–3), 357-368.

7. Zolfaghari, R.; Fakhru'l-Razi, A.; Abdullah, L. C.; Elnashaie, S. S. E. H.; Pendashteh, A., Demulsification techniques of water-in-oil and oil-in-water emulsions in petroleum industry. *Sep. Purif. Technol.* **2016,** 170, 377-407.
8. Noik, C.; Chen, J.; Dalmazzone, C. S. H., Electrostatic Demulsification on Crude Oil: A State-of-the-Art Review. In *International Oil & Gas Conference and Exhibition in China*, Society of Petroleum Engineers: Beijing, China, 2006; p 12.
9. Sams, G. W.; Zaouk, M., Emulsion Resolution in Electrostatic Processes. *Energy & Fuels* **2000,** 14, (1), 31-37.
10. Fan, Y.; Simon, S.; Sjöblom, J., Chemical Destabilization of Crude Oil Emulsions: Effect of Nonionic Surfactants as Emulsion Inhibitors. *Energy & Fuels* **2009,** 23, 4575-4583.
11. Amarzguioui, M.; Jacobsen, P. C., Novel use of Electro Coalescence to Enhance, Optimize and Debottleneck Oil Separation Trains. In *SPE Annual Technical Conference and Exhibition, 28-30 September*, Society of Petroleum Engineers: Houston, Texas, SPE-174763-MS, 2015.
12. Zhang, H.; Fang, S.; Ye, C.; Wang, M.; Cheng, H.; Wen, H.; Meng, X., Treatment of waste filature oil/water emulsion by combined demulsification and reverse osmosis. *Sep. Purif. Technol.* **2008,** 63, (2), 264-268.
13. Zhang, W.; Xiao, P.; Wang, D., Central treatment of different emulsion wastewaters by an integrated process of physicochemically enhanced ultrafiltration and anaerobic–aerobic biofilm reactor. *Bioresour. Technol.* **2014,** 159, 150-156.
14. Rajaković, V.; Skala, D., Separation of water-in-oil emulsions by freeze/thaw method and microwave radiation. *Sep. Purif. Technol.* **2006,** 49, (2), 192-196.
15. Atten, P. In *On electrocoalescence of water droplets in an insulating liquid*, The IEEE Industry Applications Society Annual Meeting, Houston, TX, USA, 4-9 Oct, 1992, IEEE.
16. Eddy, W. O. Process for treatment of oil emulsions. Patent: US1529349A. 1923.
17. Herbsman, A. M. Method of treating petroleum emulsions. US patent 931112. 1933.
18. Eddy, H. C. Method of salvaging oil from sludge. US Patent 1 826 276. 1931.
19. Cottrell, F. G.; Speed, J. B. Separating and collecting particles of one liquid suspended in another liquid. 1911.
20. Jones, T. J.; Neustadter, E. L.; Whittingham, K. P., Water-In-Crude Oil Emulsion Stability And Emulsion Destabilization By Chemical Demulsifiers. *J. Can. Pet. Technol.* **1978,** 17, (02), 100-108.
21. Aveyard, R.; Binks, B. P.; Fletcher, P. D. I.; Lu, J. R., The resolution of water-in-crude oil emulsions by the addition of low molar mass demulsifiers. *J. Colloid Interface Sci.* **1990,** 139, (1), 128-138.
22. Angle, C. W., Chemical Demulsification of Stable Crude Oil and Bitumen Emulsions in Petroleum Recovery-A Review. In *Encyclopedic Handbook of Emulsion Technology*, Sjoblom, J., Ed. Mercel Dekker: New York, 2001; pp 541-594.
23. Opedal, N. v. d. T.; Kralova, I.; Lesaint, C.; Sjöblom, J., Enhanced Sedimentation and Coalescence by Chemicals on Real Crude Oil Systems. *Energy & Fuels* **2011,** 25, (12), 5718-5728.
24. Pearce, C. A. R., The mechanism of the resolution of water-in-oil emulsions by electrical treatment. *British Journal of Applied Physics* **1954,** 5, (4), 136.
25. Berg, T. G. O.; Fernish, G. C.; Gaukler, T. A., The Mechanism of Coalescence of Liquid Drops *Journal of the atmospheric sciences* **1963,** 20, 153-158.
26. Sartor, D., A laboratory investigation of collision efficiencies, coalescence and electrical charging of simulated cloud droplets. *J. Meteorol.* **1954,** 11, 91-103.
27. Less, S.; Hannisdal, A.; Bjørklund, E.; Sjöblom, J., Electrostatic destabilization of water-in-crude oil emulsions: Application to a real case and evaluation of the Aibel VIEC technology. *Fuel* **2008,** 87, (12), 2572-2581.
28. Mhatre, S.; Simon, S.; Sjöblom, J.; Xu, Z., Demulsifier assisted film thinning and coalescence in crude oil emulsions under DC electric fields. *Chem. Eng. Res. Des.* **2018,** 134, 117-129.

29. Yang, D.; Ghadiri, M.; Sun, Y.; He, L.; Luo, X.; Lü, Y., Critical electric field strength for partial coalescence of droplets on oil–water interface under DC electric field. *Chem. Eng. Res. Des.* **2018,** 136, 83-93.
30. Kang, W.; Yin, X.; Yang, H.; Zhao, Y.; Huang, Z.; Hou, X.; Sarsenbekuly, B.; Zhu, Z.; Wang, P.; Zhang, X.; Geng, J.; Aidarova, S., Demulsification performance, behavior and mechanism of different demulsifiers on the light crude oil emulsions. *Colloids and Surfaces A: Physicochemical and Engineering Aspects* **2018,** 545, 197-204.
31. Nowbahar, A.; Whitaker, K. A.; Schmitt, A. K.; Kuo, T.-C., Mechanistic Study of Water Droplet Coalescence and Flocculation in Diluted Bitumen Emulsions with Additives Using Microfluidics. *Energy & Fuels* **2017,** 31, (10), 10555-10565.
32. Sørland, G. H. In *Characterization of Emulsions by PFG-NMR* The 10th International Bologna Conference on Magnetic Resonance in Porous Media, 12-16 September, Leipzig, Germany, 2010; Leipzig, Germany, 2010; pp 27-31.
33. Hjartnes, T. N.; Sørland, G. H.; Simon, S.; Sjöblom, J., Demulsification of Crude Oil Emulsions Tracked by Pulsed Field Gradient (PFG) Nuclear Magnetic Resonance (NMR). Part I: Chemical Demulsification. *Industrial & Engineering Chemistry Research* **2019**.
34. Taylor, S. E., Investigations into the electrical and coalescence behaviour of water-in-crude oil emulsions in high voltage gradients. *Colloids and Surfaces* **1988,** 29, (1), 29-51.
35. Eow, J. S.; Ghadiri, M.; Sharif, A. O.; Williams, T. J., Electrostatic enhancement of coalescence of water droplets in oil: a review of the current understanding. *Chem. Eng. J.* **2001,** 84, (3), 173-192.
36. Aryafar, H.; Kavehpour, H. P., Electrocoalescence: Effects of DC Electric Fields on Coalescence of Drops at Planar Interfaces. *Langmuir* **2009,** 25, (21), 12460-12465.
37. Bailes, P. J.; Kuipa, P. K. In *Resolution of emulsions using electric fields with gas sparging*, First European Congress on Chemical Engineering. The third Italian Conference on chemical and process engineering, 4-7 May, Florence, Italy, 1997; AIDIC Secretariat: Florence, Italy, 1997; pp 2861-2864.
38. Zhang, Y.; Liu, Y.; Ji, R.; Cai, B.; Li, H.; Wang, F., Dehydration Efficiency of Water-In-Model Oil Emulsions in High Frequency Pulsed DC Electrical Field: Effect of Physical and Chemical Properties of the Emulsions. *J. Dispersion Sci. Technol.* **2012,** 33, (11), 1574-1581.
39. Schlumberger More efficient dehydration and desalting with a larger operating range at lower operating temperatures. Available at: http://www.slb.com/services/processing-separation/oil-treatment/dehydration-desalting/. (22nd of May, 2017),
40. Chen, T. Y.; Mohammed, R. A.; Bailey, A. I.; Luckham, P. F.; Taylor, S. E., Dewatering of crude oil emulsions 4. Emulsion resolution by the application of an electric field. *Colloids and Surfaces A: Physicochemical and Engineering Aspects* **1994,** 83, (3), 273-284.
41. Bailes, P. J.; Larkai, S. K. L., Experimental investigation into the use of high voltage DC fields for liquid phase separation. *Transactions of the Institution of Chemical Engineers* **1981,** 59, (4), 229-237.
42. Taylor, S. E., Theory and practice of electrically-enhanced phase separation of water-in-oil emulsions. *Chem. Eng. Res. Des.* **1996,** 74, (5), 526-540.
43. Wang, B.-B.; Wang, X.-D.; Wang, T.-H.; Lu, G.; Yan, W.-M., Electro-coalescence of two charged droplets under constant and pulsed DC electric fields. *Int. J. Heat Mass Transfer* **2016,** 98, 10-16.
44. Li, B.; Sun, Z.; Wang, Z.; Jin, Y.; Fan, Y., Effects of high-frequency and high-voltage pulsed electric field parameters on water chain formation. *Journal of Electrostatics* **2016,** 80, 22-29.
45. Lesaint, C.; Glomm, W. R.; Lundgaard, L. E.; Sjöblom, J., Dehydration efficiency of AC electrical fields on water-in-model-oil emulsions. *Colloids and Surfaces A: Physicochemical and Engineering Aspects* **2009,** 352, (1), 63-69.
46. Lundgaard, L.; Berg, G.; Ingebrigtsen, S.; Atten, P., Electrocoalescence for oil-water separation: Fundamental aspects. In *Emulsions and emulsion stability*, Sjoblom, J., Ed. Taylor & Francis: 2006; Vol. 132, pp 549-592.

47. Holto, J.; Berg, G.; Lundgaard, L. E. *Electrocoalescence of Drops in a Water-in-Oil Emulsion*; SINTEF Energy Research: Trondheim, Norway, 2009.
48. Simon, S.; Nenningsland, A. L.; Herschbach, E.; Sjöblom, J., Extraction of Basic Components from Petroleum Crude Oil. *Energy & Fuels* **2009,** 24, 1043-1050.
49. Petroleum Safety Authority Norway, 2019, Available at: https://www.ptil.no/regelverk/alle-forskrifter/?forskrift=613. (30th of August, 2019),
50. SHOTT *Technical glasses: Physical and technical properties. Available at: https://www.schott.com/d/epackaging/2fbc7180-e37c-4209-9eec-617ad9208e51/1.4/final_schott_technical_glasses_row.pdf*; SHOTT: Mainz, Germany, 2014.
51. Drelich, J.; Bryll, G.; Kapczynski, J.; Hupka, J.; Miller, J. D.; Hanson, F. V., The effect of electric field pulsation frequency on breaking water-in-oil emulsions. *Fuel Process. Technol.* **1992,** 31, (2), 105-113.
52. Gorur Govinda, R., Dielectric Loss and Relaxation—I. In *Dielectrics in Electric Fields*, CRC Press: 2016.
53. Opedal, N. v. d. T.; Sørland, G.; Sjöblom, J., Methods for Droplet Size Distribution Determination of Water-in-Oil Emulsions using Low-Field NMR. *diffusion-fundamentals.org* **2009,** 9, (7), 1-29.
54. Simon, S.; Pierrard, X.; Sjöblom, J.; Sørland, G. H., Separation profile of model water-in-oil emulsions followed by nuclear magnetic resonance (NMR) measurements: Application range and comparison with a multiple-light scattering based apparatus. *J. Colloid Interface Sci.* **2011,** 356, (1), 352-361.
55. Sandnes, R.; Simon, S.; Sjöblom, J.; Sørland, G. H., Optimization and validation of low field nuclear magnetic resonance sequences to determine low water contents and water profiles in W/O emulsions. *Colloids and Surfaces A: Physicochemical and Engineering Aspects* **2014,** 441, 441-448.
56. ConocoPhillips *Eldfisk II: Videreutvikling av Eldfisk-feltet med videreført drift av Embla-feltet. Available at: http://static.conocophillips.com/files/resources/impact_assessment_eldfiskii_final.pdf*; ConocoPhillips.com, 2010.
57. Kokal, S. L., Crude Oil Emulsions: A State-Of-The-Art Review. *SPE-77497-PA* **2005,** 20, (01), 5-13.
58. Dickinson, E.; Stainsby, G., *Colloids in food.* Applied Science Publishers: London, 1982.
59. Torza, S.; Cox, R. G.; Mason, S. G.; Taylor, G. I., Electrohydrodynamic deformation and bursts of liquid drops. *Philosophical Transactions of the Royal Society of London. Series A, Mathematical and Physical Sciences* **1971,** 269, (1198), 295-319.
60. Manga, M.; Stone, H. A., Collective hydrodynamics of deformable drops and bubbles in dilute low Reynolds number suspensions. *J. Fluid Mech.* **1995,** 300, 231-263.
61. Mhatre, S.; Thaokar, R., Electrocoalescence in non-uniform electric fields: An experimental study. *Chemical Engineering and Processing: Process Intensification* **2015,** 96, 28-38.
62. Frising, T.; Noïk, C.; Dalmazzone, C.; Peysson, Y.; Palermo, T., Contribution of the Sedimentation and Coalescence Mechanisms to the Separation of Concentrated Water-in-Oil Emulsions. *J. Dispersion Sci. Technol.* **2008,** 29, (6), 827-834.
63. Barrabino, A.; Keleşoğlu, S.; Eftekhardadkhah, M.; Simon, S.; Sjöblom, J., Enhanced sedimentation and coalescence of petroleum crude oil emulsions by the new generation of environmentally friendly yellow chemicals. *J. Dispersion Sci. Technol.* **2017,** 38, (12), 1677-1686.
64. Grimes, B. A.; Dorao, C. A.; Opedal, N. V. D. T.; Kralova, I.; Sørland, G. H.; Sjöblom, J., Population Balance Model for Batch Gravity Separation of Crude Oil and Water Emulsions. Part II: Comparison to Experimental Crude Oil Separation Data. *J. Dispersion Sci. Technol.* **2012,** 33, (4), 591-598.